Original Research *Feature article*

Bioactive, full-length parathyroid hormone delivered using an adeno-associated viral vector

Alexandra M Burr[1], Pamela Cabahug Zuckerman[2,3,4], Alesha B Castillo[2,3,4], Nicola C Partridge[5] and Biju Parekkadan[1]

[1]Department of Biomedical Engineering, Rutgers, The State University of New Jersey, Piscataway, NJ 08854, USA; [2]Department of Orthopedic Surgery, NYU Langone Health, New York University, New York, NY 10016, USA; [3]Department of Biomedical Engineering, Tandon School of Engineering, New York University, New York, NY 11201, USA; [4]Rehabilitation Research and Development, Veterans Affairs New York Harbor Healthcare System, New York, NY 11209, USA; [5]Department of Molecular Pathobiology, New York University College of Dentistry, New York, NY 10010, USA
Corresponding author: Biju Parekkadan. Email: biju.parekkadan@rutgers.edu

Impact Statement

Parathyroid hormone (PTH) is critical for treatment of hypoparathyroidism. Improvements in PTH delivery are still of high interest; current PTH treatment requires repeated recombinant hormone injections and is associated with side effects and non-compliance. This work provides proof-of-concept data for using adeno-associated viral (AAV) vectors to delivery PTH as a gene therapeutic. A dose escalation study identified a systemic AAV dose that was expressed in multiple tissues, induced high levels of PTH circulating in the blood, and caused endocrine effects. By achieving levels of PTH consistent with hyperparathyroidism in mice, this dose can be translated to future evaluation of PTH gene therapy in disease models powered with therapeutic endpoints. Conversely, this study may have implications as a model to study hyperparathyroidism disease states since transgene expression allowed for continuous PTH secretion over prolonged time periods.

Abstract

Delivering the parathyroid hormone (PTH) gene has been attempted preclinically in a handful of studies, but delivering full-length PTH (1–84) using adeno-associated viral (AAV) vectors has not. Given the difficulty in achieving therapeutic levels of secreted proteins using gene therapy, this study seeks to determine the feasibility of doing so with PTH. An AAV vector was used to deliver human PTH driven by a strong promoter. We demonstrate the ability to secrete full-length PTH from various cell types *in vitro*. PTH secretion from hepatocytes was measured over time and a fluorescent marker was used to compare the secretion rate of PTH in various cell types. Potency was measured by the ability of PTH to act on the PTH receptors of osteosarcoma cells and induced proliferation. PTH showed potency *in vitro* by inducing proliferation in two osteosarcoma cell lines. *In vivo*, AAV was administered systemically in immunocompromised mice which received xenografts of osteosarcoma cells. Animals that received the highest dose of AAV-PTH had higher liver and plasma concentrations of PTH. All dosing groups achieved measurable plasma concentrations of human PTH that were above the normal range. The high-dose group also had significantly larger tumors compared to control groups on the final day of the study. The tumors also showed dose–dependent differences in morphology. When looking at endocrine signaling and endogenous bone turnover, we observed a significant difference in tibial growth plate width in animals that received the high-dose AAV as well as dose–dependent changes in blood biomarkers related to PTH. This proof-of-concept study shows promise for further exploration of an AAV gene therapy to deliver full-length PTH for hypoparathyroidism. Additional investigation will determine efficacy in a disease model, but data shown establish bioactivity in well-established models of osteosarcoma.

Keywords: Hypoparathyroidism, AAV vector, AAV-PTH, parathyroid hormone

***Experimental Biology and Medicine* 2022; 247: 1885–1897. DOI: 10.1177/15353702221097087**

Introduction

Hypoparathyroidism treatment requires daily recombinant hormone injections. Hypoparathyroidism affects around 77,000 adults in the United States.[1] It is a disease in which patients fail to produce sufficient amounts of PTH or PTH lacks activity.[2] This results in low calcium levels, elevated phosphorus in the serum, and chronically reduced bone turnover rates.[3] Patients suffer from symptoms such as fatigue, brain fog, mouth numbness, twitching in face, and insomnia.[4] The most common type of hypoparathyroidism is acquired postoperatively after thyroid or parathyroid surgery.[5]

Hypoparathyroidism is increasingly being recognized as an endocrine disorder with unmet need. One challenge is overcoming the short half-life of PTH which is measured

to be around 4 min in native form and about 2 h for rhPTH 1–84.[6,7] There are several companies adding hypoparathyroidism to their pipelines with a range of novel therapeutics from cell and gene therapies to small molecules. Drugs in development aim to reduce injection frequency, or have improved stability to be administered orally.[8]

Gene therapy for hypoparathyroidism, however, has only been attempted preclinically thus far. In one example, CMV-PTH plasmids were delivered via polymeric micelles which were orally administered to rats.[9] PTH was measured to be slightly above detection limits and calcium levels increased for four weeks postdelivery. Other groups have used plasmids, polycationic liposomes, and adenovirus to deliver the PTH transgene into various small animal models.[10–12] Adeno-associated virus (AAV) has been a widely utilized tool in gene therapy with over 150 clinical trials initiated in the last five years.[13] While AAV is not a perfect solution for gene delivery, a new industry is rising around trying to overcome the shortfalls of AAV vectors by creating designer viruses, mitigating immunogenicity, and improved purification methods.[14] Here, we propose utilizing AAV to deliver full-length human PTH. In this proof-of-concept study, we demonstrate for the first time that AAV-hPTH can be used to secrete PTH from exogenous cell types and has bioactivity in effector cells.

While the dynamicity and complexity of PTH is accepted by bone metabolism and endocrinology specialists, it is still not fully characterized and robust *in vitro* assays are lacking.[15] One fairly well-understood PTH pathway is the expression of PTH receptors (PTHR1) on osteosarcoma cells. Many studies have shown the ability of both recombinant and endogenous PTH to induce proliferation of these cell types.[15–18] In addition, rodent studies have been conducted to assess the prevalence of bone neoplasms as a result of long-term use of recombinant PTH, as human PTH has high homology with both mouse and rat PTH.[19,20] Using this principle, we show that PTH secreted from AAV-transduced cells and in mice can induce osteosarcoma cell proliferation. The potency of PTH demonstrated here using AAV vectors holds promise for further characterization as an efficacious gene therapy.

Materials and methods

AAV vector production

Human eukaryotic elongation factor 1 α1 (EF1α, 1179 bp) promoter was used along with a post-transcriptional regulatory element (WPRE, 598 bp).[12] The EF1α-PTH-WPRE plasmid was designed with the full-length (448 bp) PTH cDNA sequence (accession no. NM_001316352) and cloned into an AAV backbone (Applied Biologic Materials, Canada). The AAV-EF1α-PTH-IRES-GFP-WPRE plasmid was designed and purchased from VectorBuilder (Chicago, IL, USA). Plasmid maps for PTH plasmids can be found in the Supplementary Information. The AAV-CMV-GFP plasmid was purchased from Clontech (Mountain View, CA, USA). Rep/Cap serotype 2 and pHelper plasmids (Clontech) were used for triple plasmid cotransfection to produce virus in adherent HEK293T cells (ATCC, Manassas, VA, USA). Briefly, cells were seeded at 45% confluency (7×10^4 cells/cm^2) and allowed to adhere overnight. The Rep/Cap and Helper plasmids were combined with the AAV-EF1α-PTH plasmid at a 1:1:1 molar ratio and incubated in Opti-MEM medium with PEI (Polyplus Sciences) for 15 min to form complexes. The solution was added dropwise to cell cultures in Opti-MEM media. Media were replaced 24 h after transfection and were collected after 96 h.[21]

The supernatant was collected and filtered through a 0.22-μM filter and processed using tangential flow filtration (Pall Biotech, Port Washington, NY, USA) with a 100-kDa membrane cassette. Viral particles were resuspended in sterile phosphate-buffered saline (PBS) containing 0.01% Pluronics-F68 solution. Each batch was quantified using quantitative polymerase chain reaction (qPCR) AAV titration kit (Applied Biologic Materials) and analyzed using Quant Studio3 (Invitrogen, Waltham, MA, USA). Only batches with yields $>5 \times 10^2$ vg/cell were used for experiments. Viral solutions were stored at −80 C until use.

Cell culture and *in vitro* transduction

HepG2 hepatocytes were seeded at 25% confluence in 12-well plates and allowed to adhere overnight in Eagle's minimum essential medium (EMEM) complete (ATCC) with 10% fetal bovine serum (FBS) (GIBCO) and 1% antibiotic/antifungal. AAV vectors were added at a multiplicity of infection (MOI) of 5×10^4 and volume was brought up to 0.5 mL using antibiotic-free medium and incubated for 24 h before medium was changed to complete medium.

For cellular secretion rate, HepG2, HEK293, and U2OS cells were seeded at 25% confluence in a 12-well plate in complete medium (EMEM, Dulbecco's modified eagle medium (DMEM), and McCoy's 5A, respectively) and allowed to adhere overnight. AAV vectors were added an MOI of 5×10^4 and volume was brought up to 0.5 mL using antibiotic-free medium and incubated for 24 h before medium was changed to complete medium.

SaOS-2 cells and U2OS osteosarcoma cells were seeded at 5% confluence in 48-well plates and allowed to adhere overnight in McCoy's 5A complete with 10% FBS and 1% antibiotic/antifungal. AAV vectors were added at varying MOI. Volume was adjusted to 0.25 mL using antibiotic-free medium and incubated for 24 h. For potency assays, serum-free medium was used, and cells were subcultured weekly.

In vitro assays

A continuous-flow, culture perfusion system optimized in our lab was used as previously described.[22] In brief, a 12-well plate was modified to include plug-flow input and output streams to measure media samples at a rate of 0.2 mL per hour for 120 h. To measure transduction efficiency for all *in vitro* experiments, GFP-positive cells were counted as a percentage of total cell count using image cytometry on day 3 post-transduction (Celigo, Nexcelom, Lawrence, MA, USA). PTH secretion for HEK293, HepG2, and U2OS cells was determined by transducing cells with the AAV2-EF1a-PTH-IRES-GFP vector. PTH was measured by collecting media that was incubated for 24 h between day 3 and 4 post-transduction via enzyme-linked immunoassay (ELISA) (Applied

Biologic Materials). The ELISA detects the 84 amino acid sequence of human PTH, but cross-reactivity was not validated. Per cell secretion was determined by calculating total PTH per well divided by the number of transduced cells.

The PTH potency assay was performed by transducing osteosarcoma cell lines (SaOS-2 and U2OS) with AAV2-EF1a-PTH-IRES-GFP vectors. Supernatant from 24 h of accumulation was measured post-transduction via ELISA. Normalized proliferation was measured by tracking cell confluence over time and comparing it to the time-matched control wells which were transduced with AAV2-EF1a-GFP vectors. Confluence was quantified using brightfield image cytometry (Celigo, Nexcelom).

Experimental animals

NOD.Cg-*Prkdc*^{scid} *Il2rg*^{tm1Wjl}/SzJ (NSG) mice, aged 8–10 weeks, were used, and allowed food and water *ad libitum*. Eight male and eight female mice were assigned randomly to sex-matched AAV-dosing groups: high (5×10^{10} viral genomes), medium (1×10^{10} viral genomes), low (5×10^{9} viral genomes), and negative (5×10^{10} viral genomes AAV-GFP). All animals received 50 µL AAV solution in sterile saline via tail vein. 100-µL blood was collected 20 days post-AAV injection in heparin-coated tubes via tail vein to measure plasma PTH. Three weeks post-AAV injection, 2.5 million SaOS-2 cells were injected subcutaneously on the dorsal flank of each mouse in 100 µL. Tumor length and width was measured via digital caliper every five days postinjection until one or more tumors grew beyond 1 cm in diameter. Tumor volume was calculated as (length × width^2)/2. Mice were euthanized and tumors were extracted, imaged, measured, and weighed. Liver samples were flash-frozen in liquid nitrogen and stored at −80°C. Efficiency of AAV delivery was measured by quantifying the concentration of PTH in the liver and the number of AAV genome copies per µg of genomic DNA in the liver by qPCR. DNeasy kit was used (QIAGEN, Hilden, Germany) to extract DNA from homogenized samples. qPCR was performed using primers for the inverted terminal repeat (ITR) region on AAV as follows: 5′-GGAACCCCTAGTGATGGAGTT-3′ and 5′-CGGCCTCAGTGAGCGA-3.′ For protein extraction, CelLytic MT lysis buffer (MilliporeSigma, Burlington, MA, USA) was used.

Bone tissue collection and analysis

At the time of euthanasia, tibias were dissected and placed immediately in 10% neutral-buffered formalin solution for fixation overnight. After fixation, samples were rinsed with PBS and decalcified over 1–2 weeks. Decalcification was performed by placing samples in 20× volume of 20% w/v EDTA solution using H2O and NaOH to adjust pH to 7.4. EDTA solution was replaced twice a week until decalcification was complete when bone was soft and pliable. After decalcification, samples were paraffin embedded, sectioned, and stained with Hematoxylin and Eosin (H&E). Slides were imaged using an Evos XL Core microscope at 20×. H&E images of the tibial head were used to measure the width of the growth plate. Growth plate was identified as the epiphysial region between trabecular bone areas on images and all zones were included resting, proliferative, and hypertrophic zones. Five measurements were taken across the growth plate for each sample using ImageJ software (Java). Measurements were averaged and compared across groups.

Blood biomarker analysis

To measure the changes in bone-related proteins in the blood, plasma samples collected at euthanasia were analyzed using a Multiplex panel and Luminex xMap technology (Millipore). The Mouse Bone MAP Panel (Millipore) contained magnetic beads which can be detected with unique fluorophores for each analyte using the Luminex analyzer (MAGPIX; Luminex, Austin, TX, USA). The analytes were as follows: adrenocorticotropic hormone (ACTH), interleukin-6 (IL-6), osteoprotegerin, insulin, leptin, Dickkopf WNT signaling pathway inhibitor 1 (DKK1), sclerostin, tumor necrosis factor alpha (TNFA), and fibroblast growth factor 23 (FGF23). Each analyte was measured using an antibody-immobilized bead which was tagged with a unique magnetic bead fluorophore. The assay was performed according to the manufacturer protocol which utilized a magnetic separation block for plate washing steps, an eight-point standard curve and two quality controls. Fifty events per bead were measured from 50 µL samples. Analysis was performed using the median fluorescent intensity (MFI) data to calculate the concentrations in samples.

AAV8 osteosarcoma study

The study was repeated with AAV8 serotype vector for EF1a-PTH. Vector was produced as previously described. NSG mice, aged 8–10 weeks, were used, and allowed food and water *ad libitum*. Sixteen male mice were assigned randomly to AAV dosing groups with higher dosing this time: high (1×10^{11} viral genomes), medium (5×10^{10} viral genomes), low (1×10^{10} viral genomes), and negative (5×10^{10} viral genomes AAV-GFP). SaOS-2 injection and tumor monitoring were carried out in the same manner as the previous study.

As before, PTH concentration was measured on day 21 postinjection of AAV via ELISA and mice were euthanized 42 days postinjection of tumor cells. In this trial, endpoint blood collection was used to measure calcium, phosphorus, total procollagen type 1 N-terminal propeptide (P1NP), and C-terminal telopeptide of type 1 collagen (CTX). For the phosphorus measurement, CEDEX BioAnalyzer was used with PhosphateBio metabolite kit (Roche, Basel, Switzerland) according to the manufacturer protocol. For the calcium measurement, a calcium colorimetric assay (Abcam, Cambridge, UK) was used according to the manufacturer protocol. Briefly, 25 µL of plasma was added to each well in duplicate, assay was performed, absorbance was read via VarioSkan plate reader (Invitrogen) and concentration was calculated from a six-point standard curve. CTX and total P1NP were measured using ELISA (Immunodiagnostic Systems, East Boldon, UK) according to the manufacturer protocols. 20 and 5 µL of plasma were used in duplicate for each sample for CTX and P1NP kits, respectively.

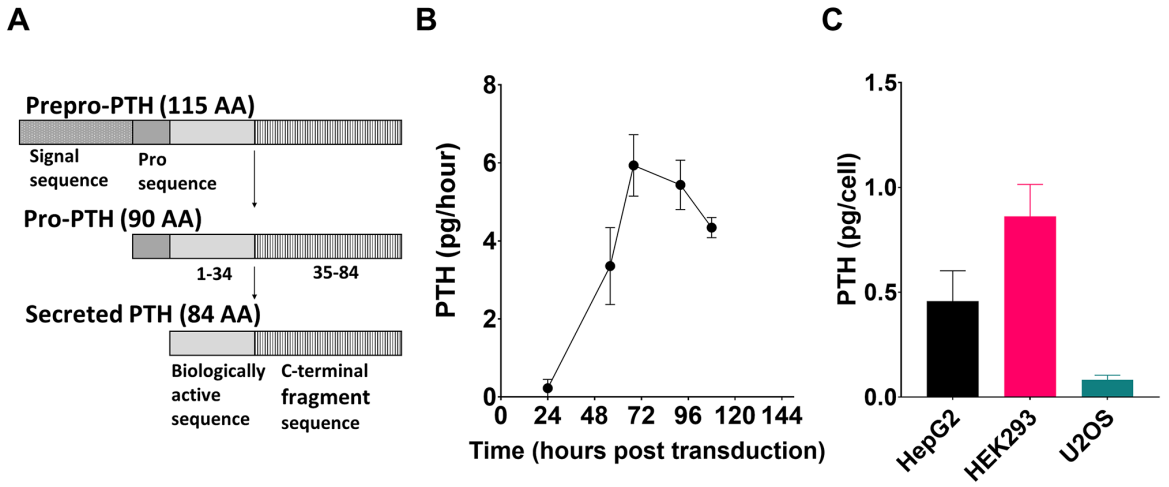

Figure 1. Exogenous cell types can be engineered to secrete PTH in vitro. (A) The AAV vector used for all experiments contains the human cDNA sequence for the full 115 residue human prepro-PTH peptide. Through endogenous post-translational modification pathways, secreted PTH is 84 amino acids in full form. (B) Kinetic secretion of PTH by HepG2 cells after transduction with AAV2-EF1α-PTH. Cells were perfused with media at 0.2 mL/h over 110 h to track secretion and expression over time. At maximal rates, 10^5 cells secreted 5 pg/h of human PTH. $N = 4$ per group. (C) Three cell lines were transduced with AAV-EF1α-PTH-IRES-GFP at an MOI of 5000. Per cell secretion rate was obtained by sampling the PTH concentration in the well at 72 h post-transduction/the number of transduced cells per well. Mean values shown are three well replicates in two experiments for total of $n = 6$ per group. Data are shown as mean values ± SD. (A color version of this figure is available in the online journal.)

Statistical analysis

Data are shown as mean value ± standard deviation for each group. All statistical analyses were performed using GraphPad Prism. For *in vitro* potency assays, a two-way analysis of variance (ANOVA) with multiple comparisons and Tukey's post hoc analysis was used to determine statistical significance ($P < 0.05$) for each group compared to the control at each timepoint. For all other analyses, one-way ANOVA with Tukey's post hoc analysis was used to determine statistical significance ($P < 0.05$) for weight and endpoint volume. Dose–dependent significance was evaluated using a one-way ANOVA for each analyte with a test for linear trend between means in left-to-right order ($P < 0.05$).

Results

In vitro transduction

The relatively short size of full-length, human PTH makes it a good candidate for transgene expression in the AAV genome. Endogenously, the 115 residue prepro-peptide is synthesized by parathyroid chief cells in the parathyroid gland. It is then translocated to the ER where it is cleaved to pro-PTH.[23] Within the trans-Golgi network, it is cleaved to PTH and either secreted or stored. The entire *de novo* synthesis is believed to last 30 min.[24] Where most of the treatments in development have focused on the 84 or 34 amino sequence for PTH, we have utilized the full-length 115 amino acid sequence which results in a secreted form which is 84 amino acids (Figure 1(A)).

Because full-length, human PTH has not been secreted previously using an AAV vector, we first sought to detect PTH from ELISA in cell cultures. A hepatocyte cell line, HepG2, was used to represent a similar cell type transduced *in vivo* when AAV is delivered systemically. Our continuous-flow perfusion system allowed for precise quantification of the secretion rate of cells over time (Figure 1(B)).[22] PTH secretion was measured over time for five days post-transduction. For each well, PTH secretion averaged about 6 pg per hour at peak expression which occurred around 72 h post-transduction.

Various cell types have different secretory capacities which may be protein dependent. To demonstrate how this may vary for PTH specifically, we compared the secretion rates of HepG2 cells to HEK293 and osteosarcoma cells (U2OS). As shown in Figure 1(C), when normalized to the number of transduced cells, HEK293 cells had the highest secretion rate of about 0.8 pg per cell per day. While there was no statistically significant difference, HepG2 had the next highest rate which was over double the rate of U2OS cells, around 0.4 pg per cell. This should be a factor when considering an administration route for gene therapy, as it shows that the cell type transduced may alter the PTH levels even after transduction efficiency has been accounted for.

In vitro potency assay

After determining that PTH can be secreted from various cell types, it is important to measure whether it is biologically active. Most *in vitro* potency assays for PTH have been on the nanogram/mL or microgram/mL scale, which may not be physiologically relevant as the normal range in human serum is 14–65 pg per milliliter.[17,18] In our potency assay, the historically chosen osteosarcoma cell lines for PTH exposure were used: SaOS-2 and U2OS. While both cell types express the parathyroid hormone receptor 1 (PTHR1), both cell types are typically used for both chemotherapy potency assays as well as PTH-related studies. It has been shown that PTHR1 expression levels vary between them, as well as their response to PTHR1-inhibiting drugs, but a few have commented on which cell line responds to PTH more effectively.[25,26]

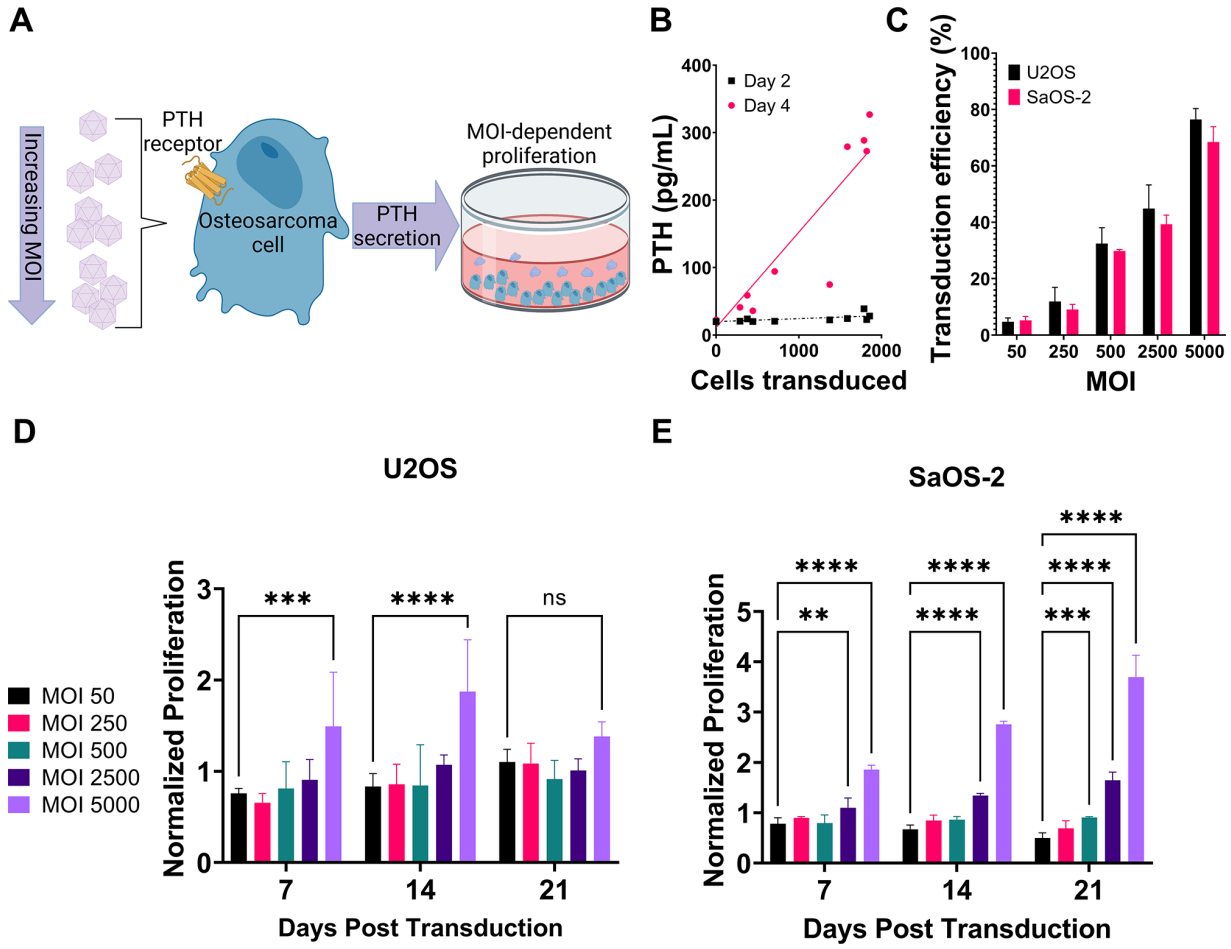

Figure 2. Secreted PTH is potent and capable of inducing osteoblast proliferation. (A) Osteosarcoma (U2OS and SaOS-2) cells were transduced with AAV-EF1α-PTH-IRES-GFP at varying multiplicity of infection (MOI). (B) The concentrations of PTH across different groups from U2OS wells correlated positively with GFP+ cell populations. (C) Transduction efficiency for each MOI and cell type as determined by GFP+ cell number compared to total cell population. Normalized proliferation of U2OS (D) and SaOS-2 (E) human osteosarcoma cell lines over time. The cells transduced at the highest MOI (5000) exhibited the highest levels of proliferation at all timepoints for both groups. Mean values shown are from four well replicates in two experiments for total of $n=8$ wells per group. Data are shown as mean values ± SD. (A color version of this figure is available in the online journal.)

To simplify the assay, U2OS and SaOS-2 cells were directly transduced so that secretion into the media would influence proliferation. To create a dose–dependent response, MOI of viral genomes (vg) per cell was increased per group (Figure 2(A)). Using a dual-expression vector that expressed both PTH and GFP, the exact number of transduced cells per well was determined. As shown in Figure 2(B), the PTH concentration in each well increased as the number of transduced cells increased, which was a product of higher MOI. PTH was measured from varying MOI groups and quantified using ELISA. Figure 2(B) shows the individual well data for MOI 5000 and 2500 vg/cell, at which the PTH was in detectable range for the assay. In addition, the 24-h accumulation concentrations were higher on day 4 post-transduction than on day 2. At the highest MOI, concentration reached upward of 300 pg/mL on day 4. Transduction efficiency was also quantified as the number of GFP-positive cells compared to total cell count on day 3 post-transduction. The percent of transduced cells was similar between cell types and increased with MOI (Figure 2(C)).

Proliferation as a function of PTH was tracked using brightfield image cytometry to quantify the percent confluence in each well. Cells were kept in serum-free media which allowed long-term growth tracking for 21 days. For both cell types, the greatest proliferation compared with the time-matched control was in the group transduced at an MOI of 5000 vg/cell and was statistically significant at all time points. Overall, SaOS-2 cells responded better since the MOI 2500 vg/cell group showed significant proliferation at days 14 and 21 while U2OS did not. In addition, SaOS-2 cells had a higher relative proliferation at around fourfold while U2OS cells were maximal at twofold. For both cell types, however, it shows that PTH secreted from osteosarcoma cells induces proliferation. It is important to note that the magnitude of 10^2 pg/mL is 10 times high than physiologic range but much lower compared to that of other studies which measure proliferation in response to PTH in the nanogram or microgram per milliliter range.[18]

AAV–PTH expression in mice

To show bioactivity of secreted PTH mediated by AAV vectors *in vivo*, an osteosarcoma tumor model was used. Subcutaneous xenografts of human SaOS-2 cells have been

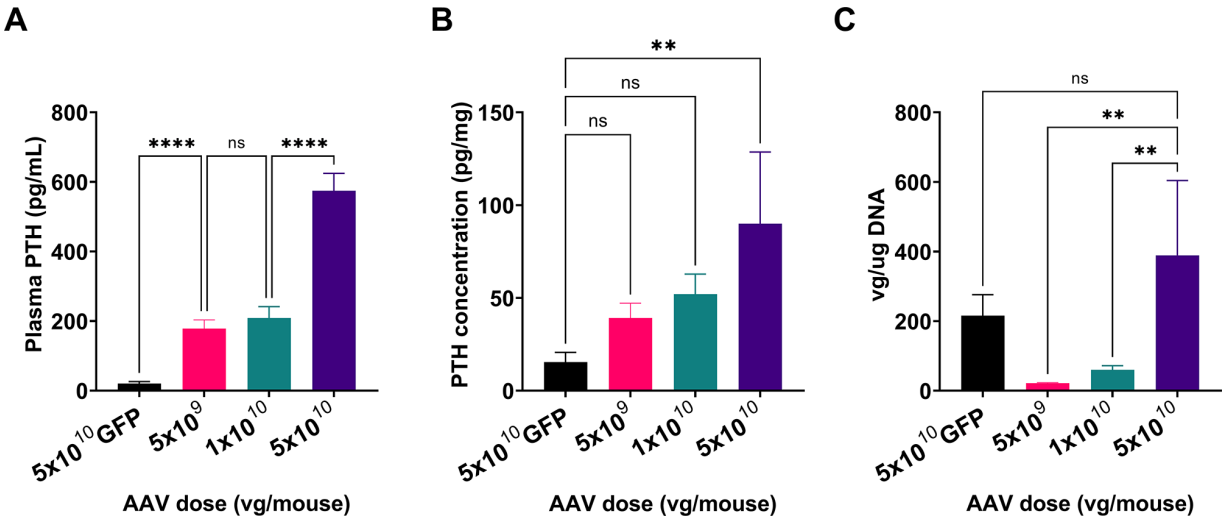

Figure 3. PTH expression in mice after AAV2 injection. (A) Plasma PTH concentrations (pg/mL) 20 days after AAV injection for each dose group. (B) Protein was extracted from liver samples after euthanasia (day 42) and measured via ELISA for PTH concentration shown as pg/mg liver tissue for each group. $N = 4$ mice per group. Data are shown as mean values ± SD. (C) AAV viral genome copies were measured in DNA extracted from liver samples using qPCR and are represented as copy number/μg genomic DNA. (A color version of this figure is available in the online journal.)
NS: non-significant.
****$P < 0.0001$.

used previously to study osteosarcoma in immunocompromised mice.[27] AAV vectors were administered intravenously via tail vein to NSG mice at varying doses of 5×10^{10}, 1×10^{10}, 5×10^{9} AAV2-EF1α-PTH vg per mouse. A control group was administered 5×10^{10} vg AAV2-CMV-GFP which served as a sham control group. SaOS-2 cells were injected three weeks post-AAV transduction. The PTH concentrations in the serum increased with AAV dose when measured the day before cell injection (day 20 postinjection), which is shown in Figure 3(A). Concentrations at this timepoint represent steady state, as it has been shown that concentrations of proteins from AAV gene therapy delivered systemically in mice at this timepoint.[28] The high-dose AAV animals had the highest concentration of PTH which was nearly a log-order higher than physiologic range. The low- and medium-dose groups had similar concentrations between 150 and 250 pg/mL. At the time of euthanasia, PTH concentration was also detected in liver sample and the highest dose group had an average of 95 pg/mg while the sham-GFP group was near or below the detection limit of the assay on average (25 pg/mg) as shown in Figure 3(B). In addition, we detected AAV viral genomes in the liver samples using primers on the ITR sequence. AAV dose correlated with the viral genome copies detected in the liver (Figure 3(C)). The high-dose PTH group had 389 vg copies/μg DNA on average while the medium- and low-dose PTH groups averaged 59.9 and 21.4 vg copies/μg DNA, respectively. The sham (GFP) group had similar concentrations to the high-dose group.

Osteosarcoma tumor growth

Due to the proliferative effect of PTH on osteosarcoma cells, the higher the PTH concentration in plasma, the faster the tumor was expected to growth compared to the sham group (GFP). The timeline for the study starting with AAV injection through euthanasia on day 42 postcell injection is shown in Figure 4(A). The tumor growth was measured using digital calipers every five days. As shown in Figure 4(B), tumors began to grow exponentially around day 20 and tumors in the high-dose group grew more aggressively than the other groups. At day 42 postcell injection, the high-dose group tumors exceeded 1 cm in diameter, so all mice were euthanized. Tumor weight-matched trends seen in tumor volume where tumors in the high-dose group weight significantly more than those in any other group (Figure 4(C)). Tumors varied in shape, size, and appearance. As shown in Figure 4(D) and (E), the low-dose group tumors were small, pale, and often contained multiple nodules. Alternatively, the high-dose tumors were larger and had more vascularization. While a dose–dependent response was not exhibited across all groups, the study does show that high levels of PTH increased tumor growth rates for the high-dose group compared to the sham group.

Effects on endogenous signaling

Bone turnover is another metric to observed PTH-induced changes. The growth plate width in rodents can be influenced by bone turnover rates because unlike humans, the epiphysial plate does not fuse in rodents. In addition, PTH treatment has been shown to increase the width of the growth plate in mice and rats.[29] PTH binds specifically to the receptors in growth plate cartilage cells. In this study, we compared the growth plate widths of the tibial head to determine if the AAV-EF1α-PTH dose affected longitudinal growth. Tibial growth plate width was measured using the ImageJ software to measure five different widths along the images of H&E sections. As shown in Figure 5(A), the growth plate width of the tibial head in animals treated with the high dose of AAV was significantly wider than any other group. Animals from the medium- and low-dose groups had growth plate widths that were not significantly

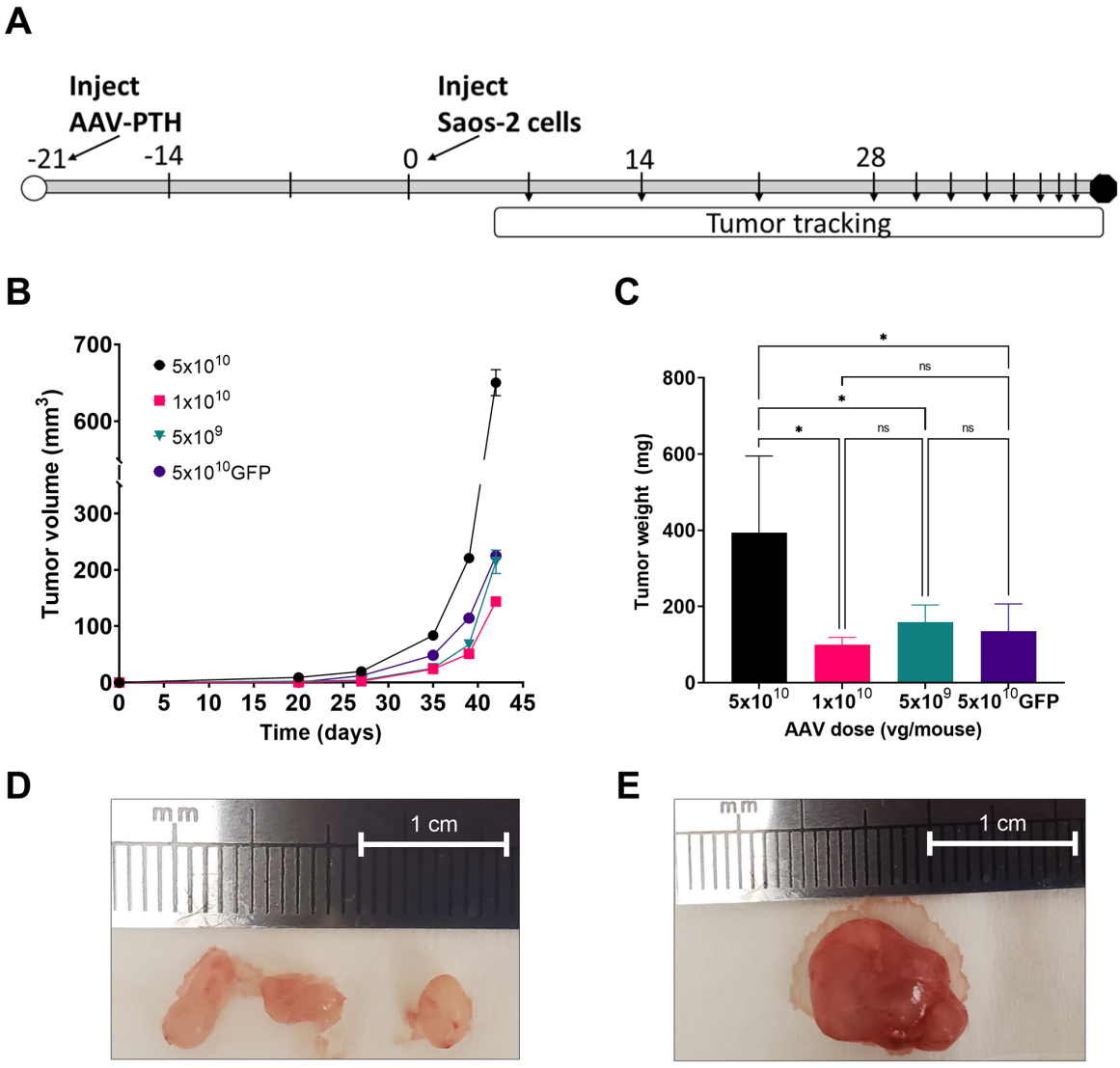

Figure 4. PTH induces tumor growth in osteosarcoma model mice. (A) Osteosarcoma model development timeline showing AAV and SaOS-2 cell injection. Arrows indicate the tumor tracking timepoints. Endpoint was day 42. (B) Tumor growth rates over time as measured by caliper showed the high-dose group grew faster than all other groups. (C) The final tumor weights for each group. Bars shown are mean values ± SD. $N = 4$ mice per group. (D) and (E) Representative images of tumors from low-dose (D) and high-dose groups (E). Scale bar shown is 1 cm in length. (A color version of this figure is available in the online journal.)

different from control animals. A representative image of the growth plate region with arrows indicating how the width was measured is shown in Figure 5(B).

Blood biomarker analysis

Given that secreted human PTH impacted bone growth in these mice, we wanted to determine if other bone turnover markers were affected. To do so, we utilized a multiplex assay that allowed quantification of nine bone-related analytes in the plasma. PTH has a complex effect on endocrine homeostasis and bone metabolism. Changes can be detected by measuring the concentration of proteins in the blood that are altered by PTH concentration. Some of these markers are directly related to PTH changes like DKK1, osteoprotegerin and sclerostin. Others are indirectly affected by PTH-induced changes in calcium reabsorption and phosphorus excretion in the kidneys or the gut. For this mechanism, PTH has been shown to influence metabolic markers such as insulin, leptin, and FGF23. Other biomarkers that are involved in PTH feedback include ACTH and inflammatory markers such as IL-6 and TNFA.

These analytes were multiplexed in a magnetic bead panel which was used to assay plasma from day 42 post-tumor cell injection (euthanasia). The results in Figure 6 show significant dose–dependent changes in blood biomarker concentrations. As shown in the top three panels (Figure 6(A) to (C)), there was a significant increase of ACTH, FGF23, and leptin concentrations in the blood with increasing AAV dose. These metabolic and endocrine responses were the most dramatic of all analytes. We show a positive correlation between AAV dose and leptin which was the most dramatic response shown ($P < 0.01$). For this biomarker, both the medium- and high-dose groups had elevated leptin levels compared to the sham controls. For the bone-specific biomarkers, we observed a variable response (Figure 6(D) to (F)). There

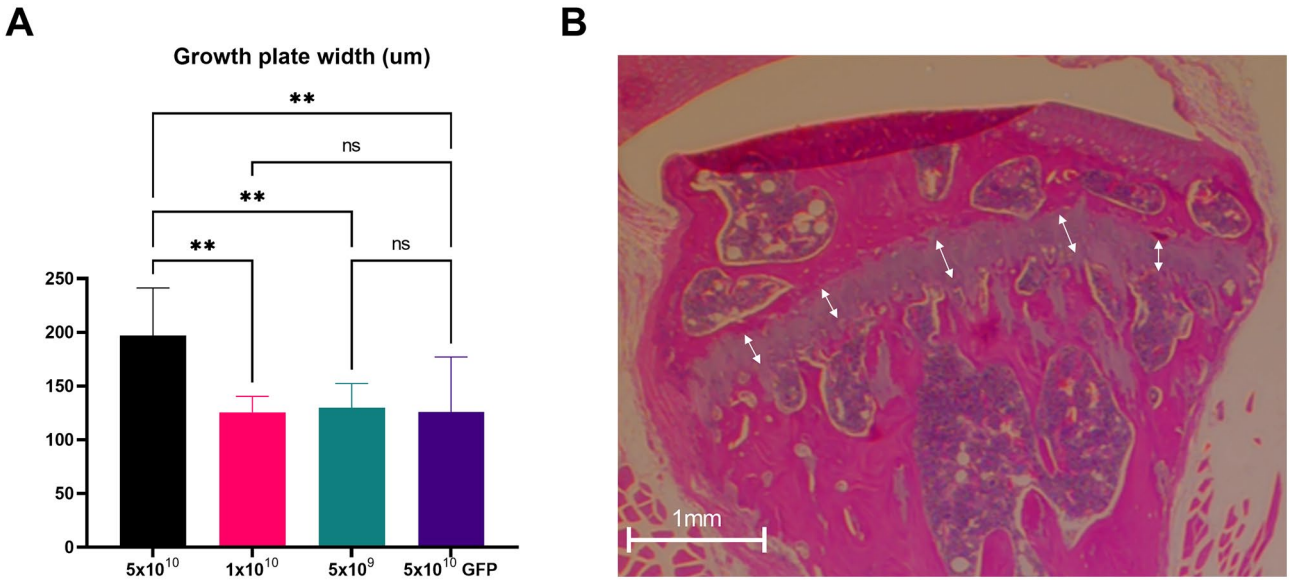

Figure 5. High-dose AAV influences growth plate width of the tibia. (A) Average growth plate width for each dosing group taken from five measurements from one H&E section from each mouse tibia. Bars represent the mean values ± SD. (B) Representative H&E images of the tibial heads from each group. (A color version of this figure is available in the online journal.)
NS: non-significant.
$^{**}P < 0.01$.

was not a significant dose-response in blood levels of sclerostin and DKK1. Interestingly, the osteoprotegerin levels in the medium-dose group were lower than the sham, and the levels were elevated in the high-dose group compared with sham controls. The final biomarkers in Figure 6(G) to (I), IL-6, insulin, and TNFA, showed variable response. For both proinflammatory markers, IL-6 and TNFA, the levels of PTH groups were all lower on average than sham controls. Finally, we measured insulin levels in the plasma. There was a significant decrease in insulin levels with increasing AAV dose, indicating a negative correlation. Interestingly, the medium-dose group had the lowest average concentration of insulin of all groups.

The biomarker analysis was used to determine the effect of PTH on endogenous endocrine signaling in the mice. Dose–dependent effects were seen in biomarkers ACTH, FGF23, leptin, insulin, and osteoprotegerin, which shows additional support for the bioactivity of human PTH secreted from AAV.

High-dose AAV8 osteosarcoma study

The results from the osteosarcoma trial show that only the highest dose of AAV2-EF1α-PTH resulted in significant effects on tumor growth in relatively small sample sizes. To determine if this phenomenon would continue with an increase in dose, the study was repeated in only male mice to minimize variation. In addition, AAV serotype 8 was used, which has been shown to achieve higher expression when injected systemically in mice. In this AAV8 study, the experimental design remained the same, but the highest dose was increased to 1×10^{11} vg/mouse.

The PTH concentration in the plasma was again measured at day 21 post-AAV injection, which is shown in Figure 7(A). The mean concentration of PTH in the 1×10^{11} vg AAV8 group was significantly higher than the medium (5×10^{10}) dose group. For dose-matched groups between studies, there was no significant different in PTH concentration between doses of AAV2 or AAV8. The PTH concentration in the GFP-sham group was undetectable by human PTH ELISA. Similarly, endpoint tumor diameter was not significantly different between the studies for dose-matched groups. The highest dose group (1×10^{11} vg) had tumors of similar size to the 5×10^{10} vg dose group, as shown in Figure 7(B). Interestingly, the liver expression as measured by qPCR was slightly higher in the AAV8 study, but not significantly different than the AAV2 study for all dose-matched groups. The highest dose AAV8 group was significantly higher than the 5×10^{10} dose group.

Given that the PTH concentrations, endpoint tumor diameters, and liver expression were similar for dose-matched groups in the AAV2 and AAV8 studies, the endpoint blood samples in this study were prioritized for measuring other blood biomarkers related to PTH signaling. First, the blood metabolites, calcium and phosphorus were measured. In states of hyperparathyroidism, calcium levels are elevated while phosphorus levels are depleted. In our AAV8 study, we observed that calcium levels did increase with dose, and the group given the highest dose had significantly higher calcium levels than controls (Figure 7(D)). Similarly, phosphorus levels decreased with increasing AAV dose, but were not significantly different than sham controls (Figure 7(E)). Finally, we measured blood markers for bone turnover. P1NP and CTX concentrations in the blood are markers of bone formation and resorption, respectively. In primary hyperparathyroidism disease states, these markers are often elevated because increased PTH acts on the signaling pathways in osteoblasts and osteoclast cells.[30] In this study, we show that increasing AAV dose and therefore PTH concentration, increased both P1NP and CTX concentrations in the blood. In Figure 7(F), P1NP was significantly elevated in all

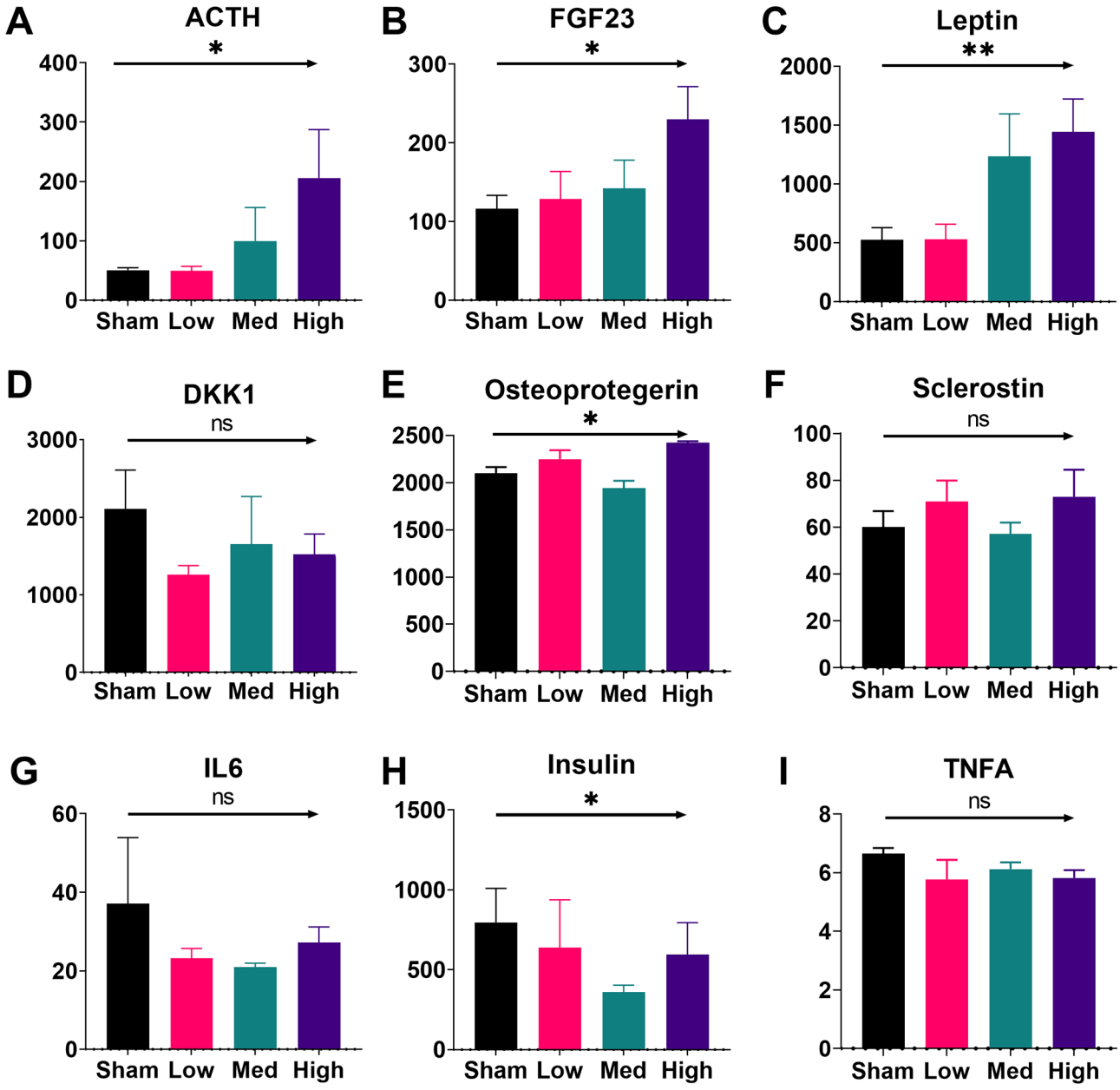

Figure 6. PTH induces dose–dependent changes in blood biomarkers. Title of each figure shows the protein analyte. Plasma samples at the time of euthanasia were used for measurement. Bars represent the mean value ± SD of animals in each group. Significance denotes a dose–dependent relationship. (A color version of this figure is available in the online journal.)
NS: non-significant; ACTH: adrenocorticotropic hormone; FGF23: fibroblast growth factor 23; DKK1: Dickkopf WNT signaling pathway inhibitor 1; IL-6: interleukin-6; TNFA: tumor necrosis factor alpha.
*$P < 0.05$; **$P < 0.01$.

PTH-dosing groups compared to the sham-GFP controls. For CTX, as shown in Figure 7(G), levels increased with dose, and were significantly different at the highest dose compared to sham controls.

Discussion

For *in vitro* assays, SaOS-2 and U2OS cells are very typically used when examining the PTH pathway. However, we have shown that the response to PTH may vary between cell types. We did not explore the mechanism of why SaOS-2 cells responded better than U2OS cells at similar MOIs, and further investigation would need to examine the PTHR1 expression levels between these cell lines at varying PTH exposure levels and timepoints. Future studies may also explore how the response of full-length PTH from AAV compares to the recombinant forms of the protein in a dose-matched manner.

One barrier to measuring PTH treatment efficacy in small animal models is the disease model available. The simplest, most representative primary hypoparathyroidism model is a parathyroidectomy. In mice, this model is not commercially available due to the high attrition rate from the difficulty to perform surgery. The next smallest animal model is rats, in

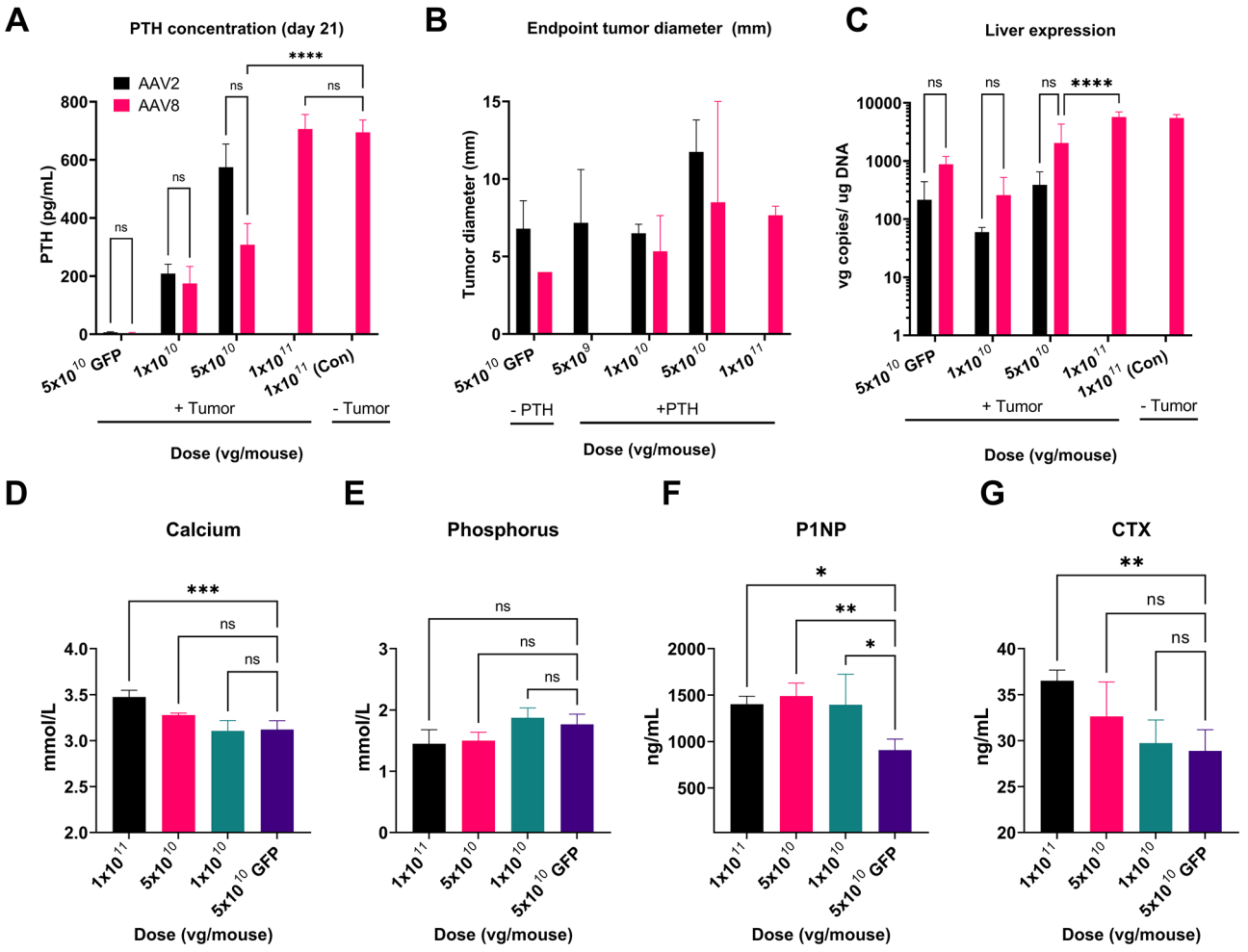

Figure 7. High-dose AAV8 osteosarcoma study. Comparative results for dose-matched groups in the AAV2 (black) and AAV8 (pink) studies for (A) PTH concentration at 21 days postinjection of AAV (pg/mL), (B) endpoint tumor diameter at day 42 postinjection of SaOS-2 cells (mm), and (C) liver expression as measured by qPCR (vg copies/μg DNA). Blood analytes for the AAV8 study for (D) calcium (mmol/L), (E) phosphorus (mmol/L), (F) P1NP, and (G) CTX. Bars represent the mean value ± SD for $n = 4$ animals/group. (A color version of this figure is available in the online journal.)
NS: non-significant.
*$P < 0.05$; **$P < 0.01$; ***$P < 0.001$; ****$P < 0.0001$.

which the surgical parathyroidectomy can be performed, but requires at least 10 times the dose of AAV vector to achieve the same dose per kilogram body weight. Using this simple cancer model, we developed a checkpoint for bioactivity of AAV-mediated PTH treatment. In addition, bioactivity of PTH using this delivery method could be applied in the future to model and study hyperparathyroidism in which continuous PTH exposure is needed. Prolonged exposure of PTH has drastically different effects than intermittent recombinant treatments, and current models of hyperparathyroidism often require osmotic pumps. AAV dose could be titrated to create varying levels of disease severity.

In this dose escalation study, we did see notable differences in gross tumor morphology. For both the low-and medium-dose groups, there were animals with multiple small tumors. Interestingly, this phenomenon was not observed in the negative control. Alternatively, the high-dose group tumors formed single, large tumors which were highly vascularized. This difference in growth has not been observed in *de novo* tumors before, but larger, repeated studies could be used to determine if the PTH concentration caused the effect.

Given that the plasma and liver concentration of PTH as well as the AAV copy number were significantly higher in the high-dose groups, we have shown that PTH concentration is causal of the osteosarcoma tumor growth in this model. However, only one timepoint was used to measure the PTH concentration in the blood, which limits the ability to draw conclusions based on long-term exposure. We assayed human PTH (1–84) but did not explore cross-reactivity with mouse PTH. The sham group dosed with GFP served as a control that exhibited normal levels of mouse PTH, which in most cases, were below the detection limit of our assay. While concentrations in other tissues were not measured, it has been shown that AAV2 and AAV8 expressions are significantly higher in the mouse liver compared with other organs when AAV is administered systemically.[31] At higher doses, other systemic effects of high levels of PTH may also become apparent. However, this model was performed in a highly immunocompromised mouse model in which the differential effects of AAV serotypes may be diminished. The lack of difference between AAV2 and AAV8 expressions at similar doses suggests that the expression in

immune privileged mice would be lower so higher doses may be needed in disease models to achieve therapeutic concentrations.

Systemic bioactivity was observed through bone growth plate width and blood biomarker analyses. Growth plate width showed the same trend as was observed in tumor growth which was that only the high-dose AAV resulted in PTH levels high enough to have a significant influence. This suggests that, like tumor growth, a certain systemic concentration of PTH must be reached to influence longitudinal bone growth. These studies were performed in adult mice, which may reduce the effects PTH can induce on growth plate width. Similar results were observed in a rat study where growth plate was significantly increased by PTH treatment in 8-week-old rats but only slightly in 30-week-old rats.[29] However, this shows that high-dose AAV resulted in PTH-induced changes not only to human tumor cell proliferation, but also the endogenous bone metabolism in these mice.

In addition, we saw linear trends in blood biomarkers with increasing AAV dose. These blood biomarkers were measured at the time of euthanasia, which was approximately nine weeks after AAV injection. The PTH effects on these pathways show that AAV injections have prolonged expression for at least nine weeks. Several of the markers were directly related to PTH pathways, while others had a response but the markers themselves are indirectly related to PTH. Because the PTH concentrations resulting from AAV doses were in excess of normal ranges, we compared the relative biomarker changes to those observed in hyperparathyroidism disease states. Human PTH has been used previously to measure bioactivity in mice and the use of sham groups provided controls to compare to baseline. Induction of hyperparathyroidism was observed in several serum protein concentrations. In reference to ACTH, we suspect that this may be partially due to the tumor growth, making it an indirect effect of elevated PTH. ACTH is involved in the hypothalamus–pituitary–adrenal axis and can become elevated in stress response and increases in cortisol. However, it has been shown in some reports that PTH stimulates steroid secretion of ACTH from adrenocortical cells.[32] We do not know if these markers are influenced by the PTH concentration alone or if the tumor cells influenced these markers.

FGF23, however, is directly related to PTH levels in the blood. In the endogenous mechanism, PTH and FGF23 are involved in a negative feedback loop, where PTH stimulates FGF23 production which then suppresses PTH production.[33] In this system, we show that PTH is stimulating FGF23 production, but because PTH is driven by an exogenous EF1α promoter, there is no inhibition of PTH production. Leptin production is also shown to be positively correlated with PTH production but is most often cited as stimulating PTH production.[34] In our system, we increased PTH production and saw increased leptin production which suggests PTH can also drive changes in this pathway.

For bone-specific biomarkers, DKK1, sclerostin, and osteoprotegerin, it important to note that these are often measured in the bone tissue rather than in the blood. Transcription of these markers may be altered locally, but not to the extent to affect systemic concentrations in blood. In a study which investigated the correlation of these biomarkers with PTH levels in patients with hyperparathyroidism, sclerostin was significantly decreased and DKK1 was significantly elevated.[35] Patients with hyperparathyroidism typically have decreased serum levels of osteoprotegerin, but it has been shown in certain studies that in instances where PTH is extremely high, osteoblasts are maximally stimulated and osteoprotegerin levels are elevated.[36] While we cannot be sure this was the response in mice, the PTH levels were over 5 and 20 times higher than the normal range in the medium- and high-dose groups, respectively. For osteoprotegerin, the variation may be explained by the PTH and osteoblast stimulation threshold where PTH levels in the medium-dose groups did not reach maximal stimulation and represent a typical hyperparathyroidism model while the high-dose group had over stimulation of osteoblast cells, and therefore increased osteoprotegerin levels.

For proinflammatory cytokines, it has been shown that patients with hyperparathyroidism have elevated levels of TNFA, but IL-6 responses are shown to be variable.[37,38] This is believed to be related to the stress response from the pathophysiology of the disease. In this study, we would expect IL-6 and TNFA levels to be elevated due to the tumor-stress response. Interestingly, there was no significant dose–dependent change in either proinflammatory cytokine.

It has been shown that patients with primary hyperparathyroidism exhibit insulin resistance and often have increased insulin concentrations and that parathyroid surgery corrects insulin levels.[39] This mechanism needs further investigation but is thought to be related to vitamin D due to the relationship between vitamin D deficiency and type 2 diabetes.[40] In models of hyperparathyroidism with 25-OH-VitD deficiency, insulin secretion is decreased, which is the trend observed in this study.[41]

Finally, in an additional osteosarcoma study, we increased the dose to 1×10^{11} with an AAV8 vector which was expected to increase expression and PTH concentration compared to the AAV2 study. Interestingly, there was no difference in expression, concentration, or tumor growth for dose-matched groups between AAV2 and AAV8 studies. This suggests that the differential effects of serotype may be suppressed in immunocompromised mice compared to immune privileged mice. We did observe significantly increased PTH concentrations and liver expression in the 1×10^{11} dose group compared to the 5×10^{10} vg/mouse. Because of this, we chose to analyze important biomarkers that are often analyzed when studying hyperparathyroidism. With comparable tumor effects and expression in the AAV2 study, we observed dose–dependent changes in calcium, phosphorus, P1NP, and CTX concentrations in the plasma in the AAV8 study. Calcium and phosphorus were related as expected, inversely. Higher PTH concentration resulted in higher calcium and lower phosphorus levels. For P1NP and CTX, both increased with increasing PTH dose, but interestingly, P1NP displayed more dramatic increases at low and medium doses compared with CTX, suggesting that PTH influences osteoblastic activity with higher sensitivity than osteoclastic. This is consistent with reports of PTH treatment that increase the

anabolic window by more drastically increasing P1NP levels compared to CTX level increases.[42]

In this study, full-length PTH was secreted from multiple cell types *in vitro*, induced osteosarcoma cell proliferation, induced tumor growth in an osteosarcoma mouse model, and included endogenous bone as well as biomarkers. This serves as a checkpoint for using AAV to measure efficacy of PTH therapy in disease model rats. In addition, it shows potency in the most-studied model of the PTH pathway: osteoblastic proliferation. By minimizing animal numbers in this dose escalation study, we provide initial evidence that could be used to inform future powering endpoints. In future studies, AAV-mediated PTH can be compared with recombinant hormone efficacy and optimized for dose studies. In conclusion, AAV-mediated full-length PTH secretion is feasible both *in vitro* and *in vivo* and demonstrates bioactivity on osteoblastic cells and systemically in mice. Based on this proof-of-concept study, AAV-mediated PTH delivery should be explored as a potential therapeutic treatment for hypoparathyroidism.

AUTHORS' CONTRIBUTIONS

A.M.B. and B.P. designed the studies. A.M.B. performed the experiments. A.M.B. and P.C.Z. analyzed the data. A.M.B., A.B.C., N.C.P., and B.P. supervised the project and assisted in study design.

ACKNOWLEDGEMENTS

The authors acknowledge the Rutgers University Research Pathology Services Core for sectioning and staining bone samples.

DECLARATION OF CONFLICTING INTERESTS

The author(s) declared the following potential conflicts of interest with respect to the research, authorship, and/or publication of this article: A patent application has been filed on the technology (PCT/US2020/020125). The authors declare no other competing financial interests.

FUNDING

The author(s) disclosed receipt of the following financial support for the research, authorship, and/or publication of this article: The research reported in this publication was supported by the National Institutes of Health: National Center for Advancing Translational Sciences of the National Institutes of Health (TL1TR003019), the National Institute of General Medicine (T32GM135141), and the National Institute of Biomedical Imaging and Bioengineering (R01EB012521 and R01EB028782). The content is solely the responsibility of the authors and does not necessarily represent the official views of the National Institutes of Health.

DATA AVAILABILITY

Reprints and permissions information is available online. Correspondence and requests for materials should be addressed to B.P.

ORCID ID

Alexandra M Burr https://orcid.org/0000-0002-7954-3619

SUPPLEMENTAL MATERIAL

Supplemental material for this article is available online.

REFERENCES

1. Powers J, Joy K, Ruscio A, Lagast H. Prevalence and incidence of hypoparathyroidism in the United States using a large claims database. *J Bone Miner Res* 2013;**28**:2570–6
2. Shoback D. Clinical practice. Hypoparathyroidism. *N Engl J Med* 2008; **359**:391–403
3. Mannstadt M, Bilezikian JP, Thakker RV, Hannan FM, Clarke BL, Rejnmark L, Mitchell DM, Vokes TJ, Winer KK, Shoback DM. Hypoparathyroidism. *Nat Rev Dis Primers* 2017;**3**:17055
4. Bilezikian JP, Khan A, Potts JT Jr, Brandi ML, Clarke BL, Shoback D, Juppner H, D'Amour P, Fox J, Rejnmark L, Mosekilde L, Rubin MR, Dempster D, Gafni R, Collins MT, Sliney J, Sanders J. Hypoparathyroidism in the adult: epidemiology, diagnosis, pathophysiology, target-organ involvement, treatment, and challenges for future research. *J Bone Miner Res* 2011;**26**:2317–37
5. Marx SJ. Hyperparathyroid and hypoparathyroid disorders. *N Engl J Med* 2000;**343**:1863–75
6. Leiker AJ, Yen TW, Eastwood DC, Doffek KM, Szabo A, Evans DB, Wang TS. Factors that influence parathyroid hormone half-life: determining if new intraoperative criteria are needed. *JAMA Surg* 2013;**148**:602–6
7. Sikjaer T, Amstrup AK, Rolighed L, Kjaer SG, Mosekilde L, Rejnmark L. PTH(1–84) replacement therapy in hypoparathyroidism: a randomized controlled trial on pharmacokinetic and dynamic effects after 6 months of treatment. *J Bone Miner Res* 2013;**28**:2232–43
8. Winer KK. Advances in the treatment of hypoparathyroidism with PTH 1-34. *Bone* 2019;**120**:535–41
9. Chou FF, Huang SC, Chang SF, Liaw J, Hung PH. Oral gene therapy for hypoparathyroidism: a rat model. *Hum Gene Ther* 2009;**20**:1344–50
10. Zhou Y, Lu BJ, Xu P, Song CF. Optimising gene therapy of hypoparathyroidism with hematopoietic stem cells. *Chin Med J (Engl)* 2005;**118**: 204–9
11. Liu D, Zhu Y, Yang C, Long J, Yao C, Li J, Wang S. Potential treatment of hypoparathyroidism with recombinant plasmids encoding preproparathyroid hormone. *J Endocrinol Invest* 2012;**35**:479–84
12. Adriaansen J, Perez P, Zheng C, Collins MT, Baum BJ. Human parathyroid hormone is secreted primarily into the bloodstream after rat parotid gland gene transfer. *Hum Gene Ther* 2011;**22**:84–92
13. Kuzmin DA, Shutova MV, Johnston NR, Smith OP, Fedorin VV, Kukushkin YS, van der Loo JCM, Johnstone EC. The clinical landscape for AAV gene therapies. *Nat Rev Drug Discov* 2021;**20**:173–4
14. Verdera HC, Kuranda K, Mingozzi F. AAV vector immunogenicity in humans: a long journey to successful gene transfer. *Mol Ther* 2020;**28**: 723–46
15. Qin L, Raggatt LJ, Partridge NC. Parathyroid hormone: a double-edged sword for bone metabolism. *Trends Endocrinol Metab* 2004;**15**:60–5
16. Poole KE, Reeve J. Parathyroid hormone—a bone anabolic and catabolic agent. *Curr Opin Pharmacol* 2005;**5**:612–7
17. Nakazawa T, Nakajima A, Shiomi K, Moriya H, Einhorn TA, Yamazaki M. Effects of low-dose, intermittent treatment with recombinant human parathyroid hormone (1–34) on chondrogenesis in a model of experimental fracture healing. *Bone* 2005;**37**:711–9
18. Saggese G, Federico G, Cinquanta L. In vitro effects of growth hormone and other hormones on chondrocytes and osteoblast-like cells. *Acta Paediatr Suppl* 1993;**82**:54–60
19. Vahle JL, Sato M, Long GG, Young JK, Francis PC, Engelhardt JA, Westmore MS, Linda Y, Nold JB. Skeletal changes in rats given daily subcutaneous injections of recombinant human parathyroid hormone (1–34) for 2 years and relevance to human safety. *Toxicol Pathol* 2002;**30**:312–21
20. Vahle JL, Long GG, Sandusky G, Westmore M, Ma YL, Sato M. Bone neoplasms in F344 rats given teriparatide [rhPTH(1–34)] are dependent on duration of treatment and dose. *Toxicol Pathol* 2004;**32**:426–38
21. Lock M, Alvira M, Vandenberghe LH, Samanta A, Toelen J, Debyser Z, Wilson JM. Rapid, simple, and versatile manufacturing of recombinant adeno-associated viral vectors at scale. *Hum Gene Ther* 2010;**21**:1259–71

22. Erickson P, Houwayek T, Burr A, Teryek M, Parekkadan B. A continuous flow cell culture system for precision cell stimulation and time-resolved profiling of cell secretion. *Anal Biochem* 2021;**625**:114213
23. Sakwe AM, Engstrom A, Larsson M, Rask L. Biosynthesis and secretion of parathyroid hormone are sensitive to proteasome inhibitors in dispersed bovine parathyroid cells. *J Biol Chem* 2002; **277**:17687–95
24. MacGregor RR, Cohn DV. The intracellular pathway for parathormone biosynthesis and secretion. *Clin Orthop Relat Res* 1978:244–58
25. Li S, Pei Y, Wang W, Liu F, Zheng K, Zhang X. Quercetin suppresses the proliferation and metastasis of metastatic osteosarcoma cells by inhibiting parathyroid hormone receptor 1. *Biomed Pharmacother* 2019;**114**:108839
26. Wen J, Qin Y, Li C, Dai X, Wu T, Yin W. Mangiferin suppresses human metastatic osteosarcoma cell growth by down-regulating the expression of metalloproteinases-1/2 and parathyroid hormone receptor 1. *AMB Express* 2020;**10**:13
27. Zhang D, Jiang F, Wang X, Li G. Knockdown of SALL4 inhibits proliferation, migration, and invasion in osteosarcoma cells. *Oncol Res* 2017;**25**:763–71
28. Zincarelli C, Soltys S, Rengo G, Rabinowitz JE. Analysis of AAV serotypes 1–9 mediated gene expression and tropism in mice after systemic injection. *Mol Ther* 2008;**16**:1073–80
29. Ogawa T, Yamagiwa H, Hayami T, Liu Z, Huang KY, Tokunaga K, Murai T, Endo N. Human PTH (1–34) induces longitudinal bone growth in rats. *J Bone Miner Metab* 2002;**20**:83–90
30. van Lierop AH, Witteveen JE, Hamdy NA, Papapoulos SE. Patients with primary hyperparathyroidism have lower circulating sclerostin levels than euparathyroid controls. *Eur J Endocrinol* 2010;**163**:833–7
31. Marsic D, Mendez-Gomez HR, Zolotukhin S. High-accuracy biodistribution analysis of adeno-associated virus variants by double barcode sequencing. *Mol Ther Methods Clin Dev* 2015;**2**:15041
32. Mazzocchi G, Aragona F, Malendowicz LK, Nussdorfer GG. PTH and PTH-related peptide enhance steroid secretion from human adrenocortical cells. *Am J Physiol Endocrinol Metab* 2001;**280**:E209–13
33. Lanske B, Razzaque MS. Molecular interactions of FGF23 and PTH in phosphate regulation. *Kidney Int* 2014;**86**:1072–4
34. Hoang D, Broer N, Sosa JA, Abitbol N, Yao X, Li F, Rivera-Molina F, Toomre DK, Roman SA, Sue G, Kim S, Li AY, Callender GG, Simpson C, Narayan D. Leptin is produced by parathyroid glands and stimulates parathyroid hormone secretion. *Ann Surg* 2017;**266**:1075–83
35. Viapiana O, Fracassi E, Troplini S, Idolazzi L, Rossini M, Adami S, Gatti D. Sclerostin and DKK1 in primary hyperparathyroidism. *Calcif Tissue Int* 2013;**92**:324–9
36. Coen G, Ballanti P, Balducci A, Calabria S, Fischer MS, Jankovic L, Manni M, Morosetti M, Moscaritolo E, Sardella D, Bonucci E. Serum osteoprotegerin and renal osteodystrophy. *Nephrol Dial Transplant* 2002;**17**:233–8
37. Ogard CG, Engelmann MD, Kistorp C, Nielsen SL, Vestergaard H. Increased plasma N-terminal pro-B-type natriuretic peptide and markers of inflammation related to atherosclerosis in patients with primary hyperparathyroidism. *Clin Endocrinol (Oxf)* 2005;**63**:493–8
38. Luboshitzky R, Chertok-Schaham Y, Lavi I, Ishay A. Cardiovascular risk factors in primary hyperparathyroidism. *J Endocrinol Invest* 2009; **32**:317–21
39. Ginsberg H, Olefsky JM, Reaven GM. Evaluation of insulin resistance in patients with primary hyperparathyroidism. *Proc Soc Exp Biol Med* 1975;**148**:942–5
40. Tai K, Need AG, Horowitz M, Chapman IM. Vitamin D, glucose, insulin, and insulin sensitivity. *Nutrition* 2008;**24**:279–85
41. Soares MJ, Ping-Delfos WC, Sherriff JL, Nezhad DH, Cummings NK, Zhao Y. Vitamin D and parathyroid hormone in insulin resistance of abdominal obesity: cause or effect? *Eur J Clin Nutr* 2011;**65**:1348–52
42. Almirol EA, Chi LY, Khurana B, Hurwitz S, Bluman EM, Chiodo C, Matzkin E, Baima J, LeBoff MS. Short-term effects of teriparatide versus placebo on bone biomarkers, structure, and fracture healing in women with lower-extremity stress fractures: a pilot study. *J Clin Transl Endocrinol* 2016;**5**:7–14

(Received January 11, 2022, Accepted April 10, 2022)